

# A Porous Coordination Polymer Assembled from 8-Connected $\{\text{Co}^{\text{II}}_3(\text{OH})\}$ Clusters and Isonicotinate: Multiple Active Metal Sites, Apical Ligand Substitution, $\text{H}_2$ Adsorption, and Magnetism

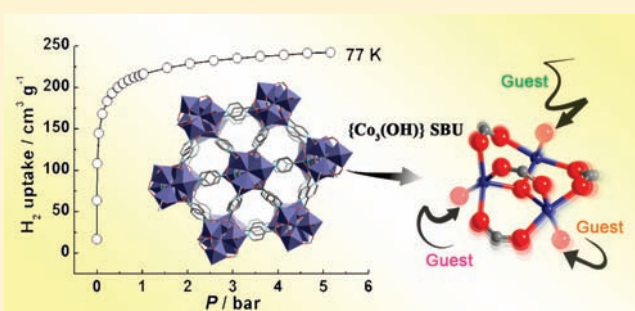
Qing Chen,<sup>†</sup> Jian-Bin Lin,<sup>†</sup> Wei Xue,<sup>†</sup> Ming-Hua Zeng,<sup>\*,†</sup> and Xiao-Ming Chen<sup>\*,†</sup>

<sup>†</sup>MOE Key Laboratory of Bioinorganic and Synthetic Chemistry/State Key Laboratory of Optoelectronic Materials and Technologies, School of Chemistry and Chemical Engineering, Sun Yat-Sen University, Guangzhou 510275, P. R. China

<sup>\*</sup>Key Laboratory of Synthetic and Natural Functional Molecule Chemistry of the Ministry of Education, Northwest University, Xi'an 710069, P. R. China

**S** Supporting Information

**ABSTRACT:** A microporous coordination polymer, namely,  $[\text{Co}_3(\text{ina})_4(\text{OH})(\text{C}_2\text{H}_5\text{OH})_3](\text{NO}_3) \cdot \text{C}_2\text{H}_5\text{OH} \cdot (\text{H}_2\text{O})_3$  (**1**, or MCF-38, ina = isonicotinate), with 8-connected  $\{\text{Co}_3(\text{OH})\}$  clusters as the structural secondary building units, has been solvothermally synthesized. The hydroxo-centered Co(II) cluster involves multiple active metal sites. The interesting apical ligand substitutions have been directly observed, and the corresponding products of  $[\text{Co}_3(\text{ina})_4(\text{OH})(\text{G})_x(\text{H}_2\text{O})_n](\text{NO}_3) \cdot \text{G} \cdot (\text{H}_2\text{O})_m$  (**1**  $\supset$  **PrOH**, G = PrOH,  $x = 2$ ,  $n = 1$ ,  $m = 3$ ; **1**  $\supset$  **BuOH**, G = BuOH,  $x = 2$ ,  $n = 1$ ,  $m = 1$ , and **1**  $\supset$  **MeOH**, G = MeOH,  $x = 3$ ,  $n = 0$ ,  $m = 7$ ) have also been obtained by solvothermal syntheses or crystal-to-crystal transformations. High-pressure  $\text{H}_2$  adsorption measurement at 77 K reveals that activated **1** can absorb 2.2 wt %  $\text{H}_2$  at 5 bar. The relative  $\text{H}_2$  absorption at low pressure (86% of the storage capacity at 1 bar) is higher than the corresponding values reported for some typical porous coordination polymers. The magnetic studies of **1** show a dominant antiferromagnetic coupling between Co(II) ions of intra- and inter-cluster.



## INTRODUCTION

The research on cluster-based coordination polymers has attracted considerable attention for their intriguing architectures and potential applications as functional materials.<sup>1–5</sup> It is considered that some fascinating properties of metal clusters can be inherited by the final structures.<sup>2,3</sup> For example, the assembly of coordination polymers by using magnetic clusters as secondary building units (SBUs) can provide an attractive route for the preparation of porous magnets,<sup>4</sup> while metal cluster units containing different terminal sites can be used not only for the rational assembly, but also for the creation of potential active sites for effective adsorption and other chemical/physical activities.<sup>5,6</sup> Therefore, the introduction of metal active sites in the porous frameworks has recently become one of the most active topics because of their beneficial role, and the accompanied apical ligand substitution reactions have also aroused interest.<sup>7,8</sup> Meanwhile, the dynamic crystal-to-crystal transformations are helpful to probe the changes that occur upon the metal active sites and the flexibility of the frameworks at the molecular level.<sup>9,10</sup> Herein, we report a new porous coordination polymer (PCP)  $[\text{Co}_3(\text{ina})_4(\text{OH})(\text{C}_2\text{H}_5\text{OH})_3](\text{NO}_3) \cdot \text{C}_2\text{H}_5\text{OH} \cdot (\text{H}_2\text{O})_3$  (**1**, or MCF-38; ina = isonicotinate), which is composed of atypical Co(II) hydroxo-centered trinuclear clusters acting as SBUs and active metal sites due to the coordinative instability of apical

EtOH molecules. The interesting apical ligand substitution of the SBUs and the solvent template effect have been studied. The  $\text{H}_2$  storage capacity and magnetic properties of **1** have also been characterized.

## EXPERIMENTAL SECTION

**Materials and General Methods.** Solvents and reagents were of reagent grade and used as received. Infrared spectra were recorded in the range 400–4000  $\text{cm}^{-1}$  on a Bruker TENSOR 27 Fourier transform infrared spectrometry (FT-IR) spectrophotometer using KBr pellets. Elemental analyses were performed on a Perkin-Elmer 2400 elemental analyzer (C, H, N). Thermogravimetry analyses (TGA) were performed on a Netzsch TG 209 instrument in flowing  $\text{N}_2$  with a heating rate of 10  $^\circ\text{C}/\text{min}$ . Powder X-ray diffraction (PXRD) measurements were performed on a Bruker D8 ADVANCE X-ray diffractometer with  $\text{Cu K}\alpha$  radiation. Variable-temperature PXRD measurements were recorded after the sample had stayed at the respective temperature for 30 min in  $\text{N}_2$  atmosphere. Gas sorption isotherms were performed with a Belsorp-Max automatic volumetric adsorption apparatus. Detailed ac and dc magnetic data were collected on a Quantum Design MPMS SQUID-XL-7 magnetometer using the crushed single crystals.

**Received:** October 2, 2010

**Published:** February 22, 2011

Table 1. Crystallographic Data

complex	1	1 ⊃ PrOH	1 ⊃ BuOH	1 ⊃ MeOH
formula	C <sub>30</sub> H <sub>43</sub> Co <sub>3</sub> N <sub>5</sub> O <sub>19</sub>	C <sub>33</sub> H <sub>49</sub> Co <sub>3</sub> N <sub>5</sub> O <sub>19</sub>	C <sub>36</sub> H <sub>51</sub> Co <sub>3</sub> N <sub>5</sub> O <sub>17</sub>	C <sub>28</sub> H <sub>47</sub> Co <sub>3</sub> N <sub>5</sub> O <sub>23</sub>
formula weight	954.5	996.6	1002.6	998.5
temperature (K)	123(2)	123(2)	123(2)	123(2)
crystal system	orthorhombic	orthorhombic	orthorhombic	orthorhombic
space group	<i>Pnma</i>	<i>Pnma</i>	<i>Pnma</i>	<i>Pnma</i>
<i>a</i> (Å)	18.986(4)	18.9542(2)	18.9705(2)	18.7824(1)
<i>b</i> (Å)	19.683(4)	19.697(2)	19.4783(2)	19.6842(1)
<i>c</i> (Å)	12.081(2)	12.0228(1)	12.0751(1)	12.0490(7)
<i>V</i> (Å <sup>3</sup> )	4514.6(2)	4488.6(8)	4461.9(7)	4454.7(5)
<i>Z</i>	4	4	4	4
<i>D<sub>c</sub></i> (g cm <sup>-3</sup> )	1.298	1.304	1.263	1.253
<i>μ</i> (mm <sup>-1</sup> )	1.150	1.157	1.156	1.162
reflns coll.	4539	4082	4055	4435
unique reflns	3713	3411	3845	3296
<i>R<sub>int</sub></i>	0.0451	0.0387	0.0327	0.0557
<i>R<sub>1</sub></i> <sup>a</sup> [ <i>I</i> > 2σ( <i>I</i> )]	0.0882	0.0967	0.0886	0.0966
w <i>R</i> <sup>b</sup> <sub>2</sub> (all data)	0.2653	0.2722	0.2417	0.2640
GOF	1.075	1.014	1.077	1.042
Δρ <sub>min/max</sub> /e (Å <sup>-3</sup> )	1.81/−2.79	1.77/−1.53	2.77/−1.83	1.35/−0.95

$$^a R_1 = \sum [|F_o| - |F_c|] / \sum |F_o|, \quad ^b wR_2 = [\sum w(F_o^2 - F_c^2)^2 / \sum w(F_o^2)]^{1/2}.$$

**Preparation of [Co<sub>3</sub>(ina)<sub>4</sub>(OH)(C<sub>2</sub>H<sub>5</sub>OH)<sub>3</sub>](NO<sub>3</sub>)·C<sub>2</sub>H<sub>5</sub>OH·(H<sub>2</sub>O)<sub>3</sub> (1).** A mixture of Co(NO<sub>3</sub>)<sub>2</sub>·6H<sub>2</sub>O (1 mmol, 0.029 g), Hina (1 mmol, 0.121 g), triethylamine (0.20 mL), and EtOH (10 mL) was sealed in a 15 mL Teflon-lined stainless-steel parr bomb at 140 °C for 72 h, which was then slowly cooled to room temperature. The block red crystals were obtained in about 75% yield based on Co. Anal. Calcd for C<sub>32</sub>H<sub>47</sub>Co<sub>3</sub>N<sub>5</sub>O<sub>19</sub>: C, 39.12; H, 4.82; N, 7.13%. Found: C, 39.10; H, 4.82; N, 7.12%. IR for 1 (KBr, cm<sup>-1</sup>): 3372s, 1617s, 1550s, 1384vs, 1229w, 1058w, 1019w, 869w, 775 m, 690 m, 568w, 457w.

**Preparation of [Co<sub>3</sub>(ina)<sub>4</sub>(OH)(H<sub>2</sub>O)(C<sub>3</sub>H<sub>7</sub>OH)<sub>2</sub>](NO<sub>3</sub>)·C<sub>3</sub>H<sub>7</sub>OH·(H<sub>2</sub>O)<sub>3</sub> (1 ⊃ PrOH) and [Co<sub>3</sub>(ina)<sub>4</sub>(OH)(H<sub>2</sub>O)(C<sub>4</sub>H<sub>9</sub>OH)<sub>2</sub>](NO<sub>3</sub>)·C<sub>4</sub>H<sub>9</sub>OH·(H<sub>2</sub>O) (1 ⊃ BuOH).** The same synthetic procedure of 1 was performed with *n*-PrOH and *n*-BuOH (10 mL) instead of EtOH to generate 1 ⊃ PrOH and 1 ⊃ BuOH (Yield: about 55% and about 50% based on Co), respectively. Anal. Calcd for C<sub>33</sub>H<sub>49</sub>Co<sub>3</sub>N<sub>5</sub>O<sub>19</sub> (1 ⊃ PrOH): C, 39.77; H, 4.95; N, 7.03%. Found: C, 39.07; H, 4.57; N, 7.50%. Anal. Calcd for C<sub>36</sub>H<sub>51</sub>Co<sub>3</sub>N<sub>5</sub>O<sub>17</sub> (1 ⊃ BuOH): C, 43.13; H, 5.13; N, 6.99%. Found: C, 43.01; H, 4.83; N, 7.21%. IR data for 1 ⊃ PrOH (KBr, cm<sup>-1</sup>): 3371s, 2961 m, 2938 m, 2874w, 1622s, 1551s, 1499w, 1385vs, 1229w, 1091 m, 1058w, 1018w, 867w, 832w, 776 m, 711 m, 690s, 574w, 454w. For 1 ⊃ BuOH: 3371s, 2957 m, 2930 m, 2870w, 1625s, 1552s, 1499w, 1385vs, 1229w, 1107 m, 1060w, 1019w, 867w, 844 m, 776 m, 690s, 574w, 453w.

**Preparation of [Co<sub>3</sub>(ina)<sub>4</sub>(OH)(CH<sub>3</sub>OH)<sub>3</sub>](NO<sub>3</sub>)·CH<sub>3</sub>OH·(H<sub>2</sub>O)<sub>7</sub> (1 ⊃ MeOH).** After immersing clean crystals of 1 in MeOH solvent in small tubes at room temperature for one day, the crystals retained their primary well-defined external shapes, furnishing crystals of 1 ⊃ MeOH. Anal. Calcd for C<sub>28</sub>H<sub>47</sub>Co<sub>3</sub>N<sub>5</sub>O<sub>23</sub> (1 ⊃ MeOH): C, 33.68; H, 4.74; N, 7.01%. Found: C, 32.95; H, 4.57; N, 7.04%. IR for 1 ⊃ MeOH (KBr, cm<sup>-1</sup>): 3371s, 2925 m, 2854w, 1620s, 1550s, 1404s, 1385vs, 1229w, 1058w, 1019w, 869w, 775 m, 710 m, 690s, 578w.

**X-ray Crystallography.** Diffraction intensities of all compounds were collected on a Bruker Apex CCD area detector diffractometer (Mo Kα, λ 0.71073 Å). Absorption corrections were applied by using the multiscan program SADABS.<sup>11</sup> The structures were solved with direct methods and refined with a full-matrix least-squares technique with the SHELXTL program package.<sup>12</sup> All nonhydrogen atoms were refined

with anisotropic displacement parameters. The solvent molecules in the compounds were disordered and located from difference maps. The organic hydrogen atoms were generated geometrically (C–H 0.96 Å). Some of the ina ligands and coordinated alcohol molecules were treated with disorder models of two equivalent parts. The large *U*<sub>eq</sub>(max)/*U*<sub>eq</sub>(min) of the nonsolvent C atoms are attributed to the weakly coordinated alcohol molecules. The disordered guest molecules and nitrate anions cannot be modeled and were treated by the SQUEEZE routine,<sup>13</sup> and their amount was determined by TGA results and elemental analyses. The crystal data and structure refinement results are listed in Table 1, while the selected bond distances and bond angles are listed in Table S1 of the Supporting Information.

## RESULTS AND DISCUSSION

**Crystal Structures.** There are one and one half Co(II) ions (two independent modes), two ina ligands, half of a hydroxyl group, and one and one half EtOH molecules in an asymmetric unit of 1. Each six-coordinate Co(II) ion lies in an octahedral environment, which is formed by three carboxylate O atoms [Co–O 2.050(5)–2.080(4) Å] and one pyridyl N atom [Co–N 2.138(7)–2.218(8) Å] from four ina ligands, one μ<sub>3</sub>-O atom [Co–O 2.114(4), 2.114(6) Å], and one weakly coordinated EtOH molecule [Co–O 2.165(9), 2.176(7) Å] (Figure 1A and Figure S1 of the Supporting Information). The counter nitrate anions and some solvent molecules are located in the crystal lattice. Each Co(II) atom is linked to two other Co(II) atoms by mixed hydroxyl and syn–syn carboxylate bridges [Co···Co 3.641(1), 3.461(1) Å, Co–O–Co 118.8(2)°, 110.5(2)°] into a triangular Co<sub>3</sub>(μ<sub>3</sub>-OH)(O<sub>2</sub>C)<sub>4</sub> SBU.<sup>14</sup> Different from the reported planar {M<sub>3</sub>O} unit with equilateral triangular arrangement of D<sub>3h</sub> symmetry,<sup>6,15</sup> the central oxygen atom in the SBU of 1 is displaced from the Co<sub>3</sub> isosceles triangle to furnish an approximate C<sub>s</sub> symmetry for the {Co<sub>3</sub>O} unit.

In 1, the trinuclear SBU acts as an 8-connected node of atypical twisted dodecahedral geometry (Figure 1B). These SBUs are

further interlinked by *ina* linkers into a uninodal 8-connected hex net, in which the center-to-center distances of adjacent  $\{\text{Co}_3\text{O}(\mu_3\text{-OH})\}$  clusters are 12.083(5) and 12.081(9) Å in the *bc* plane and 9.494(8) Å along the *a* direction (Figure 1C, Table 3). Generally, small clusters with a high number of

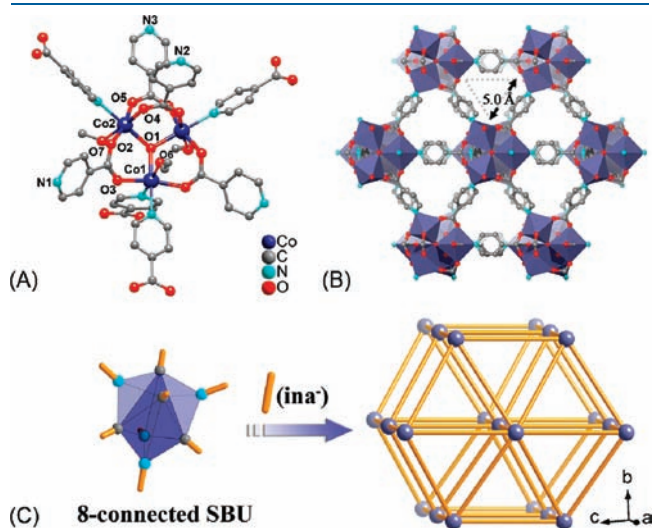


**Figure 1.** Perspective views of the coordination environment (A) and coordination framework (B) of **1** along the *a* axis (counteranions and H atoms omitted for clarity). Schematic representation of the uninodal 8-connecting twisted dodecahedral node and the hex topological net of **1** (C).

### Scheme 1. Distribution of Numbers of Connection of Polynuclear SBUs with Different Nuclear Numbers in 3-D Coordination Polymers

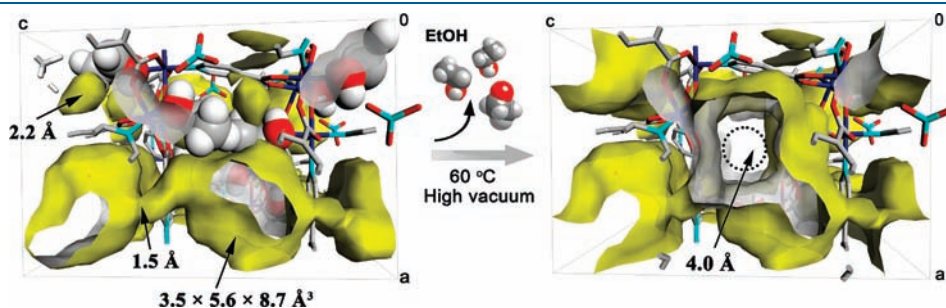
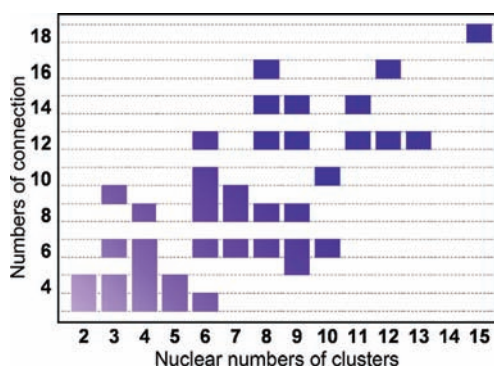


**Figure 2.** Perspective views of the cavity and channel in **1** (left), and the possible transformation upon desorption of coordinated EtOH molecules, in which the weakly coordinated EtOH are highlighted in space-filling modes (right).

connections are limited because of the steric effect,<sup>1,2,16</sup> whereas high connectivity nodes (more than six) are often made up by bulk high-nuclear metal clusters (usually higher than hexanuclear) (Scheme 1).<sup>2,3a</sup> The trinuclear clusters of the type  $\text{M}_3(\mu_3\text{-OH})(\text{O}_2\text{CR})_n\text{L}_m$  ( $\text{M} = \text{Cr}, \text{Fe}, \text{Ni}, \text{Co}, \text{etc.}$ ) have been widely used as 3-connected, octahedral and trigonal-prismatic 6-connected SBUs,<sup>6,15</sup> but only one tricapped trigonal-prismatic uninodal 9-connected node has been reported recently.<sup>17</sup> To the best of our knowledge, **1** is the first case of the 8-connected net based on the above hydroxo-centered trinuclear SBUs, and also represents the smallest unit in the known 8-connected net.<sup>2</sup>

The void space of **1** consists of cavities and 1-D channels, which accommodates uncoordinated guest molecules and occupies about 19.8% volume of the crystal (Figure 2).<sup>18</sup> The cavity is enclosed by the apical ligands in SBUs and adjacent nitrate anion, with an internal free diameter of about 2.2 Å. The 1-D channels running along the *a* axis are generated by interconnection of irregular cavities (about  $3.5 \times 5.6 \times 8.7 \text{ \AA}^3$ ), with the smallest aperture of 1.5 Å, corresponding to the trigonal window along the *a* direction with side length of about 5.0 Å (Figure 1B) (taking into account the van der Waals radii). It should be noted that the removal of all the apical coordinated EtOH molecules opens new space connecting the cavities and channels along the *b* axis by the windows with a minimum diameter of about 4.0 Å, and the free volume is then increased to 39.0% (Figure 2). The presence of potential metal active sites encouraged us to further explore the corresponding structural changes through apical ligand substitution and the porosity of this system.

**Thermal Stability.** The TGA curve (Figure 3) of **1** displays that the weight losses of the guest and coordinated solvent molecules are not well resolved. The first step from 30 to 70 °C with about 9.0% weight loss may be attributed to the release of guest EtOH and water molecules (step I, weight about 10.1%), and then that of 15.0% corresponds to the loss of three coordinated EtOH molecules up to ~200 °C (step II, about 14.1%). The PXRD patterns (Figures S2 and S3 of the Supporting Information) show that the patterns below 70 °C are almost the same, indicating that the framework is maintained after the removal of guest molecules. Between 70 and 200 °C, the decrease in intensity and slight shift of some peaks of the PXRD pattern imply that the framework is gradually distorted and/or partially collapses due to the transformation after the loss of coordinated EtOH molecules.<sup>10a</sup> Above 200 °C, the sample becomes amorphous, as shown by the absence of diffraction peaks in the PXRD pattern. The TGA performed on the desolvated sample (**1'**) after gas sorption experiments shows no significant weight loss (~2%) up to 200 °C, confirming that all uncoordinated and coordinated solvents are removed from the pores. Interestingly, the original

PXRD pattern of **1** can be recovered by immersing **1'** in fresh EtOH for several hours (Figure S2e of the Supporting Information). This dynamic phenomenon suggests a reversible structural transformation in response to the removal and adsorption of guest molecules, which indicates the framework flexibility of **1**. Unfortunately, we cannot obtain the crystal structures of the desolvated sample **1'** and resolvated sample **1''** because of their poor single crystallinity. The TGA curve of **1''** shows a similar weight loss process (inset of Figure 3), which further confirms the reversibility of the framework.

**Apical Ligand Substitutions of **1**, **1** ⊃ PrOH, **1** ⊃ BuOH, and **1** ⊃ MeOH.** Enlightened by the volatile terminal EtOH molecules and framework flexibility of **1**, we have performed crystallographic studies on the apical ligand substitution at the metal centers through different solvent-templated syntheses and crystal-to-crystal transformations.

When the similar synthetic procedure of **1** was performed with *n*-PrOH or *n*-BuOH instead of EtOH, the corresponding products of  $[\text{Co}_3(\text{ina})_4(\text{OH})(\text{H}_2\text{O})(\text{C}_3\text{H}_7\text{OH})_2](\text{NO}_3) \cdot \text{C}_3\text{H}_7\text{OH} \cdot (\text{H}_2\text{O})_3$  (**1** ⊃ PrOH) or  $[\text{Co}_3(\text{ina})_4(\text{OH})(\text{H}_2\text{O})(\text{C}_4\text{H}_9\text{OH})_2](\text{NO}_3) \cdot \text{C}_4\text{H}_9\text{OH} \cdot (\text{H}_2\text{O})$  (**1** ⊃ BuOH) (Figure 4 and Figure S5 of the Supporting Information) were yielded. However, a similar solvothermal reaction failed to give a methanol-solvated complex and

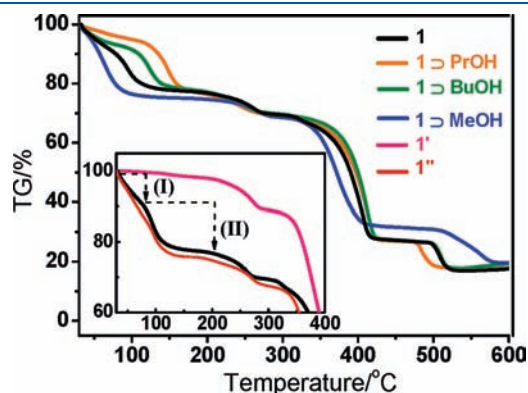
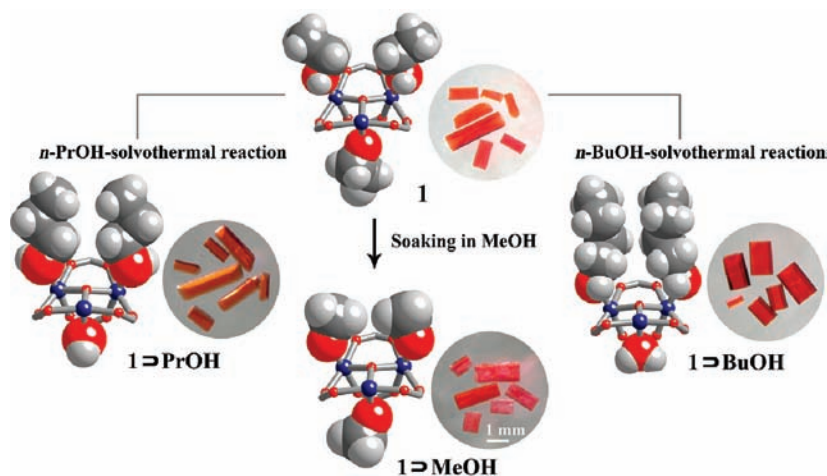


**Figure 3.** TGA curves of the four different solvate compounds, desolvated sample **1'** and resolvated sample **1''**; two steps of weight losses of **1** are indicated.

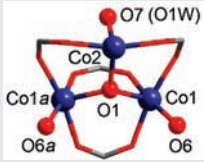
only cobalt formate as the final product. Fortunately, we successfully obtained  $[\text{Co}_3(\text{ina})_4(\text{OH})(\text{CH}_3\text{OH})_3](\text{NO}_3) \cdot (\text{CH}_3\text{OH})_2 \cdot (\text{H}_2\text{O})_7$  (**1** ⊃ MeOH) by a crystal-to-crystal transformation procedure with the mother single crystals of **1** immersed in MeOH for one day at room temperature. On the other hand, our trials by the same procedure with *n*-PrOH or *n*-BuOH as the solvent did not yield **1** ⊃ PrOH or **1** ⊃ BuOH.

As shown in Figure 4, the single crystals of the four compounds display no evident changes in size, morphology, color, or transparency. Although the crystal system and space group remain unchanged, the unit-cell volumes are decreased from 4514.6(2) to 4454.7(5) Å<sup>3</sup> in the order of **1**, **1** ⊃ PrOH, **1** ⊃ BuOH, and **1** ⊃ MeOH (Table 1). Very minor changes in the frameworks have also been observed. Slightly different from the structure of **1**, both organic solvent and water molecules participate in coordination with the Co(II) ions. Crystallographic analysis reveal that the apical site of Co1 on the mirror plane is occupied by one water molecule, while that of Co2 is bound with one PrOH or BuOH molecule in **1** ⊃ PrOH and **1** ⊃ BuOH. On the other hand, all the apical sites are occupied by MeOH molecules in **1** ⊃ MeOH. Meanwhile, all of the apical alcohol and water molecules are weakly bonded with the relatively longer Co–O distances (2.14–2.18 Å, Figure S1 of the Supporting Information), implying that they are labile in certain extent. The largest deviations in the Co–O–Co angles and Co···Co lengths within the  $\{\text{Co}_3(\text{OH})\}$  core are 2.1% for the four compounds (Table 2), which suggest the similarity of the  $\{\text{Co}_3(\text{OH})\}$  cores. In addition, the largest deviations in three types of the center-to-center distances between adjacent  $\{\text{Co}_3(\text{OH})\}$  clusters are 0.3, 0.5, and 1.1% (Table 3), respectively, which suggest marked robustness of the host frameworks.

The difference in the differently solvated products may be explained by the following considerations. First, the formation of **1**, **1** ⊃ PrOH, and **1** ⊃ BuOH may be dependent upon the presence of bulky solvent molecules that serve as templates in the solvothermal syntheses,<sup>14</sup> and such phenomenon is confirmed by the unsuccessful synthesis using smaller MeOH molecules as the solvent. Second, substitutions of the apical water and alcohol at different sites on the  $\{\text{Co}_3(\text{OH})\}$  core may be governed by the different environment around it. The larger *n*-PrOH and *n*-BuOH molecules are difficult to approach the spatially crowded

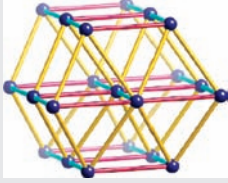


**Figure 4.** Evolution of the coordination environment of the active metal sites from ligation of EtOH molecules in **1** to other different apical ligands and the photos of their crystals.

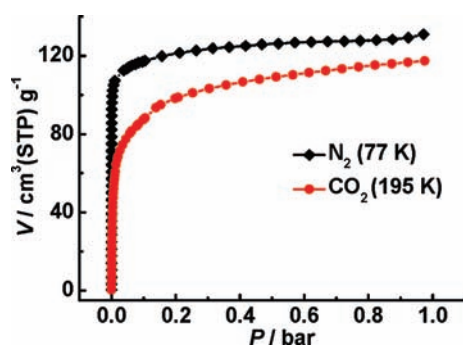
Table 2. Inter-Atomic Distances (Å) and Angles (deg) in the {Co<sub>3</sub>(OH)} Core<sup>a</sup>


	1	1 ⊃ PrOH	1 ⊃ BuOH	1 ⊃ MeOH	max deviation (%)
Co(1)–O(6)	2.176(7)	2.152(7)	2.147(5)	2.180(6)	1.5
Co(2)–O(7)	2.165(9)	—	—	2.154(7)	0.5
Co(2)–O(1W)	—	2.150(8)	2.141(7)	—	0.4
Co(1)–O(1)	2.114(3)	2.094(3)	2.101(3)	2.096(3)	0.9
Co(2)–O(1)	2.114(6)	2.107(6)	2.118(5)	2.074(4)	2.1
Co(2)···Co(1)	3.641(1)	3.613(1)	3.627(1)	3.628(1)	0.7
Co(1)···Co(1a)	3.461(1)	3.436(1)	3.423(1)	3.445(1)	1.1
Co(2)–O(1)–Co(1)	118.90(2)	118.66(2)	118.54(2)	118.94(1)	0.3
Co(1)–O(1)–Co(1a)	109.9(3)	110.3(2)	109.1(2)	110.5(2)	1.3

<sup>a</sup>Symmetry code: (a) *x*, *−y* + <sup>3</sup>/<sub>2</sub>, *z*.

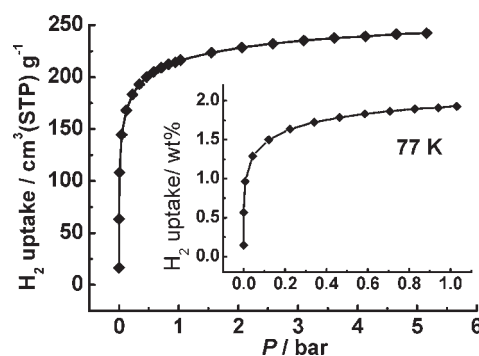
Table 3. Center–Center Distances (Å) of {Co<sub>3</sub>(OH)} Clusters in the Hex Nets


	1	1 ⊃ PrOH	1 ⊃ BuOH	1 ⊃ MeOH	max deviation (%)
type A (in blue)	9.494(8)	9.481(8)	9.500(8)	9.400(8)	1.1
type B (in yellow)	12.083(5)	12.040(5)	12.043(4)	12.074(4)	0.3
type C (in red)	12.081(9)	12.023(9)	12.075(7)	12.049(7)	0.5

Figure 5. N<sub>2</sub> and CO<sub>2</sub> adsorption isotherms.

Co1 site when compared with the water molecule, whereas the size effect seems insignificant between MeOH and water molecules yet.<sup>10a</sup> At the same time, the limited size (5.0 Å) of the triangular windows in **1** prevents the entrance of bulky guest molecules (*n*-PrOH or bigger ones) for a direct crystal-to-crystal transformation by solvent exchange.<sup>10a</sup>

**Sorption Properties.** The desolvated framework was generated by heating **1** at 60 °C for 7 h under high vacuum. N<sub>2</sub>

Figure 6. H<sub>2</sub> adsorption isotherm for **1**. Inset: enlargement of the low-pressure region.

adsorption isotherms of activated **1** at 77 K (Figure 5) present a type-I isotherm with an apparent Langmuir surface area of 544 m<sup>2</sup> g<sup>−1</sup>. The adsorption amount of N<sub>2</sub> at saturation is about 125 cm<sup>3</sup> (STP) · g<sup>−1</sup>, and the given microporous volume is *V<sub>f</sub>* = 0.20 cm<sup>3</sup>/g, lower than the *V<sub>p</sub>* value calculated from the crystal structure (0.30 cm<sup>3</sup> · g<sup>−1</sup>, void: 39.0%) using PLATON.<sup>12</sup> This is possibly due to the slight shrinkage and/or partial collapse of

**Table 4. Summary of H<sub>2</sub> Adsorption for Some PCPs at 77 K**

materials	S (m <sup>2</sup> /g) <sup>a</sup>	N (wt %) <sup>b</sup>	P (bar) <sup>c</sup>	n <sup>d</sup> (%)	ref
MIL-102	42 <sup>L</sup>	0.85/1.0	1/35	85	6e
HKUST-1	1958 <sup>L</sup>	2.18/3.6	1/50	61	7h
IRMOF-6	3263 <sup>L</sup>	1.46/4.63	1/45	32	5c
IRMOF-11	2337 <sup>L</sup>	1.6/3.5	1/34	46	5c
IRMOF-20	4346 <sup>L</sup>	1.2/6.7	1/80	19	5c
MOF-5	4400 <sup>L</sup>	1.3/5	1/80	26	5c
MOF-177	5640 <sup>L</sup>	1.2/7.1	1/66	17	5c
MOF-74	1132 <sup>L</sup>	1.6/2.3	1/26	69	5c
MOF-505	1830 <sup>L</sup>	2.47	1	—	7e
NOTT-100	1640 <sup>B</sup>	2.59/4.02	1/20	64	7b
NOTT-101	2316 <sup>B</sup>	2.52/6.05	1/20	42	7b
NOTT-102	2942 <sup>B</sup>	2.24/6.07	1/20	37	7b
Ni <sub>3</sub> (OH)(dcpyp) <sub>3</sub>	1553 <sup>B</sup>	2.0/4.15	1/20	48	6d
[Cu(dccptp)(NO <sub>3</sub> ) <sub>3</sub> ]	268 <sup>B</sup>	1.27/1.9	1/20	67	22c
PCN-12	2425 <sup>L</sup>	3.05	1	—	7c
<b>1</b>	544 <sup>L</sup>	1.9/2.2	1/5	86	this work

<sup>a</sup> Langmuir (L) or BET (B) surface area. <sup>b</sup> Amount of H<sub>2</sub> adsorbed at 77 K. <sup>c</sup> Pressure conditions, corresponding to the above N. <sup>d</sup> Relative H<sub>2</sub> adsorption at low pressure [ $n = N$  (uptake of H<sub>2</sub> at 1 bar)/N (maximum uptake of H<sub>2</sub>)]; dcpyp = 3,5-di(4-carboxyphenyl)pyridine; dccptp = 3,5-dicyano-4-(4-carboxyphenyl)-2,2':6,6''-terpyridine.

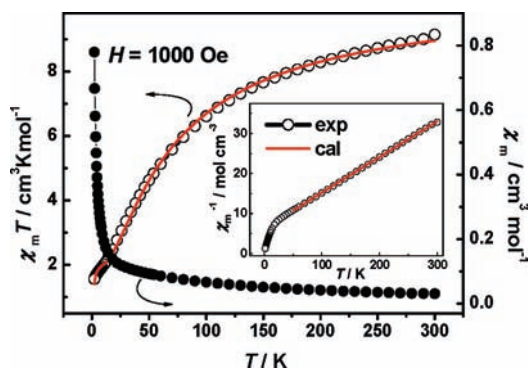


**Figure 7.** Temperature dependence of magnetic susceptibility of **1** under a static field of 1000 Oe.

the coordination framework after removing all coordinated and lattice solvents.

A high-pressure H<sub>2</sub> adsorption isotherm of **1** at 77 K (Figure 6) exhibits an increase in the adsorbed amount of hydrogen gas as the pressure up to approximately 5 bar, where the H<sub>2</sub> uptake is 242 cm<sup>3</sup> (STP)·g<sup>-1</sup>. The density of the adsorbed H<sub>2</sub> is roughly estimated with respect to V<sub>p</sub> to give a value of about 0.072 g cm<sup>-3</sup>, corresponding to that of liquid H<sub>2</sub> (0.071 g cm<sup>-3</sup>),<sup>19</sup> implying a very high degree of H<sub>2</sub> compressed in the pores.<sup>22c</sup> The adsorption enthalpy for H<sub>2</sub> is around 7.4 kJ mol<sup>-1</sup>, which is higher than that of MOF-5 (5.2 kJ mol<sup>-1</sup>) (Figure S5 of the Supporting Information). Although the maximum uptake of H<sub>2</sub> is relatively low in comparison to other PCPs with the high capacity reported to date (3.44–7.52 wt %),<sup>20</sup> the performance of **1** at low pressures compares favorably with the literature examples. The H<sub>2</sub> uptake of 1.9 wt % at 1 bar is appreciably higher than the value of microporous zeolites and aluminophosphates,<sup>20</sup> but lower than that of MOF-505, [Cu<sub>2</sub>(bptc)] or PCN-12, which show high capacities of H<sub>2</sub>

uptake (2.5–3.0 wt %) under similar conditions (77 K and 1 bar).<sup>20</sup> Significantly, 86% of the H<sub>2</sub> storage capacity of **1** at 1 bar has been reached, higher than the corresponding values of the best PCPs (Table 4).<sup>21a,22</sup> The enhancement of H<sub>2</sub> uptake can probably be attributed to the multiple open metal sites in **1**, which strengthen the H<sub>2</sub>-framework interactions. This conclusion is in accord with some investigations of strong interactions of H<sub>2</sub> with open Cu(II), Ni(II), and light metal centers.<sup>7</sup> The framework flexibility of **1** may also be responsible for the high H<sub>2</sub> storage density.

Meanwhile, CO<sub>2</sub> sorptions were also performed at 195 K (Figure 5), showing relatively low adsorption amount 117 cm<sup>3</sup> (STP)·g<sup>-1</sup> at 1 bar. A high-pressure, the CO<sub>2</sub> adsorption isotherm at 298 K (Figure S7 of the Supporting Information) exhibits an adsorption amount of 68 cm<sup>3</sup> (STP)·g<sup>-1</sup> at about 19 bar. The difference in adsorption amounts between N<sub>2</sub> and CO<sub>2</sub> gases should be better elucidated by their molecular sizes (CO<sub>2</sub> 3.4 × 3.3 × 5.4 Å<sup>3</sup>, N<sub>2</sub> 3.1 × 3.1 × 4.0 Å<sup>3</sup>) rather than the kinetic diameters (CO<sub>2</sub> 3.3 Å, N<sub>2</sub> 3.6 Å).<sup>17</sup>

**Magnetic Studies.** Magnetic susceptibility measurements were carried out on a phase pure sample of **1** with 1000 Oe. The χ<sub>m</sub>T product of each Co<sub>3</sub> unit (9.14 cm<sup>3</sup> K mol<sup>-1</sup>) at 300 K is larger than that (5.63 cm<sup>3</sup> K mol<sup>-1</sup>) expected for three magnetically isolated high-spin Co(II) atoms with S = 3/2 (Figure 7). This is a common phenomenon for Co(II) ions because of its strong spin-orbit coupling interaction.<sup>14,23</sup> The χ<sub>m</sub>T value decreases gradually with a decrease in temperature, reaching a minimum value of 1.55 cm<sup>3</sup> K mol<sup>-1</sup> at 2 K. Between 50 and 300 K, the χ<sub>m</sub><sup>-1</sup> versus T data can be well fit by the Curie-Weiss law with C = 11.9(4) cm<sup>3</sup> K mol<sup>-1</sup> and θ = -70.08(6) K. The negative θ value, which is significantly larger than those of other known Co(II)-hydroxy compounds (Table S2 of the Supporting Information),<sup>24</sup> indicates a dominating intra-cluster antiferromagnetic coupling. To further investigate the low-temperature magnetic properties of **1**, ac magnetic measurements were performed. The temperature dependence of zero-static field ac magnetic susceptibility exhibits a behavior analogous to that of dc magnetic susceptibility without frequency dependence and peaks. Even with temperatures down to 2 K, no sharp transition indicative of magnetic order has been observed. The isothermal magnetization experiments at 2 K shows the maximum magnetization of 2.83 Nβ at 70 kOe, and no magnetic hysteresis loop was observed in this system, indicating a traditional antiferromagnetic behavior.<sup>25</sup>

In order to estimate the strength of the antiferromagnetic exchange interactions, the noncritical-scaling theory with the following simple phenomenological equation was used to fit the experimental data from 300 to 2 K<sup>26</sup>

$$\chi T = A \exp(-E_1/kT) + B \exp(-E_2/kT)$$

Here, A + B equals the Curie constant, while E<sub>1</sub> and E<sub>2</sub> represent the “activation energies” corresponding to the spin-orbit coupling and the antiferromagnetic exchange interactions. This equation adequately describes the spin-orbit coupling, which results in a splitting between discrete levels. It is in excellent agreement with the experimental data obtained in this work (Figure 3). The obtained values of A + B = 10.4 cm<sup>3</sup> K mol<sup>-1</sup> and E<sub>1</sub>/k = +41.9 K (using a least-squares fitting method) are consistent with those given in the literature for the Curie constant (C ~ 11.19 cm<sup>3</sup> K mol<sup>-1</sup>) and for the effect of

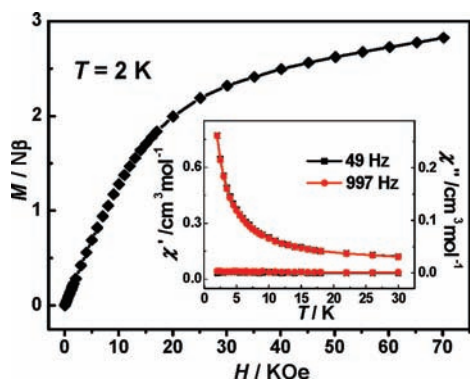


**Figure 8.** Isothermal magnetization for **1** at 2 K. Insets: temperature dependence of ac susceptibility at various frequencies.

spin-orbit coupling and site distortion ( $E_1/k$  of the order of +100 K).<sup>21</sup> As for the value found for the antiferromagnetic exchange interaction, it is weak but significant ( $E_2/k = 2.17$  K).

Usually, the bulk magnetic behaviors are consistent with the cooperative correlation of the distribution of trinuclear clusters in 3-D net, modulated by the organic bridges. The magnetic behavior of **1** is interpreted as dominated by the intra-cluster antiferromagnetic coupling because the distances between clusters are large enough to preclude any effective coupling between them. Therefore, the magnetic behavior of **1** (Figure 8) is not much different from that of similar discrete  $\text{Co}_3$  molecular systems.<sup>24b</sup>

## CONCLUSION

In summary, the  $\text{Co(II)}$  PCP based on 8-connected  $\{\text{Co}_3(\text{OH})\}$  clusters and isonicotinate linkers provides a good example for the indirect observation of interesting apical ligand substitution of active metal sites by utilizing solvothermal syntheses with different solvents and crystal-to-crystal transformations induced by guest exchanges. Three EtOH molecules weakly coordinated with the  $\{\text{Co}_3(\text{OH})\}$  core are volatile upon external stimuli. The activated **1** shows a relatively high  $\text{H}_2$  adsorption at low pressure. The investigation of **1** implies that the multiple metal active sites of the SBUs may improve the performance of PCPs, and the utilization of longer and bulky organic linkers is expected to be more profitable for gas storage.

## ASSOCIATED CONTENT

**S Supporting Information.** Selective bonds and angles, additional structural plots, PXRD, TGA curves, additional information about gas adsorption, as well as X-ray crystallographic files in CIF format. This material is available free of charge via the Internet at <http://pubs.acs.org>.

## AUTHOR INFORMATION

### Corresponding Author

\*E-mail: [zmh@nwu.edu.cn](mailto:zmh@nwu.edu.cn) (M.-H.Z.), [cxm@mail.sysu.edu.cn](mailto:cxm@mail.sysu.edu.cn) (X.-M.C.).

## ACKNOWLEDGMENT

This work was supported by NSFC (Grants 20821001, 91022015, 90922031) and the "973 Project" (Grant 2007CB815302).

## REFERENCES

- (1) Batten, S. R.; Neville, S. M.; Turner, D. R. *Coordination Polymers Design, Analysis and Application*; The Royal Society of Chemistry: London, 2009; pp 273–372.
- (2) (a) Yaghi, O. M.; O'Keeffe, M.; Ockwig, N. W.; Chae, H. K.; Eddaoudi, M.; Kim, J. *Nature* 2003, 423, 705–714. (b) Tranchemontagne D. J.; Mendoza-Cortés, J. L.; O'Keeffe, M.; Yaghi, O. M. *Chem. Soc. Rev.* 2009, 38, 1257–1283. (c) Perry, J. J., IV; Perman, J. A.; Zaworotko, M. J. *Chem. Soc. Rev.* 2009, 38, 1400–1417.
- (3) (a) Zeng, M.-H.; Zou, H.-H.; Hu, S.; Zhou, Y.-L.; Du, M.; Sun, H.-L. *Cryst. Growth Des.* 2009, 9, 4239–4242. (b) Li, J.-R.; Timmons, D. J.; Zhou, H.-C. *J. Am. Chem. Soc.* 2009, 131, 6368–6369. (c) Cairns, A. J.; Perman, J. A.; Wojtas, L.; Kravtsov, V. C.; Alkordi, M. H.; Eddaoudi, M.; Zaworotko, M. J. *J. Am. Chem. Soc.* 2008, 130, 1560–1561. (d) Sudik, A. C.; Côté, A. P.; Wong-Foy, A. G.; O'Keeffe, M.; Yaghi, O. M. *Angew. Chem., Int. Ed.* 2006, 45, 2528–2533. (e) Wang, Z.-Q.; Kravtsov, V. C.; Zaworotko, M. J. *Angew. Chem., Int. Ed.* 2005, 44, 2877–2880.
- (4) (a) Cheng, X.-N.; Zhang, W.-X.; Lin, Y.-Y.; Zheng, Y.-Z.; Chen, X.-M. *Adv. Mater.* 2007, 19, 1494–1498. (b) Wang, Z.-M.; Zhang, B.; Fujiwara, H.; Kobayashi, H.; Kurmoo, M. *Chem. Commun.* 2004, 416–417. (c) Hou, L.; Zhang, W.-X.; Zhang, J.-P.; Xue, W.; Zhang, Y.-B.; Chen, X.-M. *Chem. Commun.* 2010, 46, 6311–6313. (d) Wang, X.-F.; Zhang, Y.-B.; Xue, W.; Qi, X.-L.; Chen, X.-M. *CrystEngComm* 2010, 12, 3834–3839. (e) Cheng, X.-N.; Xue, W.; Zhang, W.-X.; Chen, X.-M. *Chem. Commun.* 2010, 46, 246–248. (f) Cheng, X.-N.; Xue, W.; Chen, X.-M. *Eur. J. Inorg. Chem.* 2010, 3850–3855.
- (5) (a) An, J.; Geib, S. J.; Rosi, N. L. *J. Am. Chem. Soc.* 2010, 132, 38–39. (b) Nouar, F.; Eubank, J. F.; Bousquet, T.; Wojtas, L.; Zaworotko, M. J.; Eddaoudi, M. *J. Am. Chem. Soc.* 2008, 130, 1833–1835. (c) Wong-Foy, A. G.; Matzger, A. J.; Yaghi, O. M. *J. Am. Chem. Soc.* 2006, 128, 3494–3495.
- (6) (a) Férey, G.; Mellot-Draznié, C.; Serre, C.; Millange, F.; Dutour, J.; Surblé, S.; Margiolaki, I. *Science* 2005, 309, 2040–2043. (b) Liu, Y.; Eubank, J. F.; Cairns, A. J.; Eckert, J.; Kravtsov, V. C.; Luebke, R.; Eddaoudi, M. *Angew. Chem., Int. Ed.* 2007, 46, 3278–3283. (c) Ma, S.; Wang, X.-S.; Manis, E. S.; Collier, C. D.; Zhou, H.-C. *Inorg. Chem.* 2007, 46, 3432–3434. (d) Jia, J.-H.; Lin, X.; Wilson, C.; Blake, A. J.; Champness, N. R.; Hubberstey, P.; Walker, G.; Cussen, E. J.; Schröder, M. *Chem. Commun.* 2007, 840–842. (e) Surblé, S.; Millange, F.; Serre, C.; Düren, T.; Latroche, M.; Bourrelly, S.; Llewellyn, P. L.; Férey, G. *J. Am. Chem. Soc.* 2006, 128, 14889–14896.
- (7) (a) Lin, J.-B.; Zhang, J.-P.; Chen, X.-M. *J. Am. Chem. Soc.* 2010, 132, 6654–6656. (b) Lin, X.; Telepeni, I.; Blake, A. J.; Dailly, A.; Brown, C. M.; Simmons, J. M.; Zoppi, M.; Walker, G. S.; Thomas, K. M.; Mays, T. J.; Hubberstey, P.; Champness, N. R.; Schröder, M. *J. Am. Chem. Soc.* 2009, 131, 2159–2171. (c) Xiang, S.-C.; Zhou, W.; Zhang, Z.-J.; Green, M. A.; Liu, Y.; Chen, B.-L. *Angew. Chem., Int. Ed.* 2010, 49, 4615–4618. (d) Wang, X.-S.; Ma, S.; Forster, P. M.; Yuan, D.; Eckert, J.; López, J. J.; Murphy, B. J.; Parise, J. B.; Zhou, H.-C. *Angew. Chem., Int. Ed.* 2008, 47, 7263–7266. (e) Chen, B.-L.; Ockwig, N. W.; Millward, A. R.; Contreras, D. S.; Yaghi, O. M. *Angew. Chem., Int. Ed.* 2005, 44, 4745–4749. (f) Forster, P. M.; Eckert, J.; Chang, J.-S.; Park, S.-E.; Férey, G.; Cheetham, A. K. *J. Am. Chem. Soc.* 2003, 125, 1309–1312. (g) Mulfort, K. L.; Wilson, T. M.; Wasielewski, M. R.; Hupp, J. T. *Langmuir* 2009, 25, 503–508. (h) Chui, S.; Lo, S.; Charmant, J.; Orpen, A.; Williams, I. *Science* 1999, 283, 1148–1150.
- (8) (a) Hwang, Y. K.; Hong, D.-Y.; Chang, J.-S.; Jung, S. H.; Seo, Y.-K.; Kim, J.; Vimont, A.; Daturi, M.; Serre, C.; Férey, G. *Angew. Chem., Int. Ed.* 2008, 47, 4144–4148. (b) Britt, D.; Furukawa, H.; Wang, B.; Glover, T. G.; Yaghi, O. M. *Proc. Natl. Acad. Sci. U. S. A.* 2009, 106, 20637–20640.
- (9) Kawano, M.; Fujita, M. *Coord. Chem. Rev.* 2007, 251, 2592.
- (10) (a) Zeng, M.-H.; Hu, S.; Chen, Q.; Xie, G.; Shuai, Q.; Gao, S.-L.; Tang, L.-Y. *Inorg. Chem.* 2009, 48, 7070–7079. (b) Das, M. C.; Bharadwaj, P. K. *J. Am. Chem. Soc.* 2009, 131, 10942–10949. (c) Zheng, S.-L.; Vande Velde, C. M. L.; Messerschmidt, M.; Volkov, A.

Gembicky, M.; Coppens, P. *Chem.—Eur. J.* 2008, 14, 706–713. (d) Takaoka, K.; Kawano, M.; Tominaga, M.; Fujita, M. *Angew. Chem., Int. Ed.* 2005, 44, 2151–2154. (e) Chen, C.-L.; Goforth, A. M.; Smith, M. D.; Su, C.-Y.; zur Loye, H.-C. *Angew. Chem., Int. Ed.* 2005, 44, 6673–6677.

(11) SHELXTL, version 6.12; Bruker Analytical Instrumentation: Madison, WI, 2000.

(12) Spek, A. L. *J. Appl. Crystallogr.* 2003, 36, 7–13.

(13) Sheldrick, G. M. SADABS, version 2.05; University Göttingen: Göttingen, Germany, 2002.

(14) Chen, Q.; Zeng, M.-H.; Wei, L.-Q.; Kurmoo, M. *Chem. Mater.* 2010, 22, 4328–4334.

(15) (a) Sudik, A. C.; Côté, A. P.; Yaghi, O. M. *Inorg. Chem.* 2005, 44, 2998–3000. (b) Zhang, X.-M.; Zheng, Y.-Z.; Li, C.-R.; Zhang, W.-X.; Chen, X.-M. *Cryst. Growth Des.* 2007, 7, 980–983. (c) Zheng, Y.-Z.; Tong, M.-L.; Xue, W.; Zhang, W.-X.; Chen, X.-M.; Grandjean, F.; Long, G. J. *Angew. Chem., Int. Ed.* 2007, 46, 6076–6080.

(16) Férey, G. J. *Solid State Chem.* 2000, 152, 37–48.

(17) Zhang, Y.-B.; Zhang, W.-X.; Feng, F.-Y.; Zhang, J.-P.; Chen, X.-M. *Angew. Chem., Int. Ed.* 2009, 48, 5287–5290.

(18) Spek, A. L. *J. Appl. Crystallogr.* 2003, 36, 7–13.

(19) *CRC Handbook of Chemistry and Physics*, 74th ed.; CRC Press: Boca Raton, FL, 1993.

(20) (a) Jhung, S. H.; Toon, J. W.; Kim, H. K.; Chang, J.-S. *Bull. Korean Chem. Soc.* 2005, 26, 1075–1078. (b) Jhung, S. H.; Toon, J. W.; Kimand, H. K.; Chang, J.-S. *J. Phys. Chem. B* 2006, 110, 9371–9374.

(21) (a) Murray, L. J.; Dincă, M.; Long, J. R. *Chem. Soc. Rev.* 2009, 38, 1294–1314. (b) Furukawa, H.; Yaghi, O. M. *J. Am. Chem. Soc.* 2009, 131, 8875–8883.

(22) (a) Pan, L.; Sander, M. B.; Huang, X.-Y.; Li, J.; Smith, M.; Bittner, E.; Bockrath, B.; Johnson, J. K. *J. Am. Chem. Soc.* 2004, 126, 1308–1309. (b) Pan, L.; Parker, B.; Huang, X. Y.; Olson, D. H.; Lee, J.; Li, J. *J. Am. Chem. Soc.* 2006, 128, 4180–4181. (c) Yang, W.-B.; Lin, X.; Jia, J.-H.; Blake, A. J.; Wilson, C.; Hubberstey, P.; Champness, N. R.; Schröder, M. *Chem. Commun.* 2008, 359–361.

(23) (a) Chen, Q.; Zeng, M.-H.; Zhou, Y.-L.; Zou, H.-H.; Kurmoo, M. *Chem. Mater.* 2010, 22, 2114–2119. (b) Zeng, M.-H.; Yao, M.-X.; Liang, H.; Zhang, W.-X.; Chen, X.-M. *Angew. Chem., Int. Ed.* 2007, 46, 1832–1835. (c) Zhou, Y.-L.; Wu, M.-C.; Zeng, M.-H.; Liang, H. *Inorg. Chem.* 2009, 48, 10146–10150.

(24) (a) Yao, M.-X.; Zeng, M.-H.; Zou, H.-H.; Zhou, Y.-L.; Liang, H. *Dalton Trans.* 2008, 2428–2432. (b) Zheng, Y.-Z.; Tong, M.-L.; Zhang, W.-X.; Chen, X.-M. *Chem. Commun.* 2006, 165–167. (c) Forster, P. M.; Burbank, A. R.; Livage, C.; Férey, G.; Cheetham, K. *Chem. Commun.* 2004, 368–369. (d) Kumagai, H.; Akita-Tanaka, M.; Inoue, K.; Kurmoo, M. *J. Mater. Chem.* 2001, 11, 2146–2151.

(25) Carlin, R. L. *Magnetochemistry*; Springer-Verlag: Berlin, 1986.

(26) (a) *Magnetism: Molecules to Materials*; Miller, J. S., Drillon, M., Eds.; Wiley-VCH: Weinheim, Germany, 2005; Vol. 5, Chapter 10, p 347. (b) Drillon, M.; Panissod, P.; Rabu, P.; Souletie, J.; Ksenofontov, V.; Gütllich, P. *Phys. Rev. B: Condens. Matter. Mater. Phys.* 2002, 65, 104404/1–104404/8.